



OPEN ACCESS

EDITED BY

Joseph Malinzi,
University of Eswatini, Eswatini

REVIEWED BY

Rendani Netshikweta,
University of Limpopo, South Africa
Bushra Majeed,
York University, Canada
Bernard Afful,
Utah State University, United States

*CORRESPONDENCE

Hatson John Boscoh Njagarah
✉ njagarahh@biust.ac.bw

RECEIVED 15 December 2025
REVISED 30 January 2026
ACCEPTED 30 January 2026
PUBLISHED 20 February 2026

CITATION

Raphaladi L, Sigauke M, Njagarah HJB
and Nedev Z (2026) Analysis of
mitigation strategies for respiratory
syncytial virus: perspectives from
mathematical modeling.
Front. Appl. Math. Stat. 12:1767887.
doi: 10.3389/fams.2026.1767887

COPYRIGHT

© 2026 Raphaladi, Sigauke, Njagarah and
Nedev. This is an open-access article
distributed under the terms of the
[Creative Commons Attribution License
\(CC BY\)](https://creativecommons.org/licenses/by/4.0/). The use, distribution or
reproduction in other forums is
permitted, provided the original author(s)
and the copyright owner(s) are credited
and that the original publication in this
journal is cited, in accordance with
accepted academic practice. No use,
distribution or reproduction is permitted
which does not comply with these terms.

Analysis of mitigation strategies for respiratory syncytial virus: perspectives from mathematical modeling

Lone Raphaladi¹, Morelyn Sigauke¹,
Hatson John Boscoh Njagarah^{1*} and Zhivko Nedev²

¹Department of Mathematics and Statistical Sciences, Botswana International University of Science and Technology, Palapye, Botswana, ²Department of Computing and Informatics, Botswana International University of Science and Technology, Palapye, Botswana

Respiratory Syncytial Virus (RSV) continues to pose a serious threat to global health, especially for young children, older adults, and people with weakened immune systems. Despite its impact, no vaccine has been licensed to prevent the disease, and there are many unanswered questions about the most effective ways to contain its spread, particularly when it comes to non-pharmaceutical measures. In this study, we developed a detailed mathematical model that captures the RSV transmission dynamics, including the often-overlooked roles of asymptomatic and post-symptomatic individuals. The model was comprehensively analyzed to confirm its well-posedness and analytical solutions, the basic reproduction number (\mathcal{R}_0) was determined, and used to determine whether the disease will fade out or persist in a population. Sensitivity analysis was performed using the Latin Hypercube Sampling (LHS) scheme to determine the factors that strongly influence the disease severity. Our findings show that reducing close contact between people, through measures like physical distancing or improved hygiene, has the greatest influence in containing the disease spread. On the other hand, efforts like widespread screening and isolating asymptomatic individuals only make a noticeable difference if contact rates are kept stable, and even then, their effect is limited. Simulations further revealed that early action is key where introducing preventive measures at the start of an outbreak can delay and lower the peak, easing pressure on healthcare systems. These insights suggest that public health policies should prioritize early, broad-based interventions and long-term solutions like vaccination over labor-intensive isolation strategies.

KEYWORDS

contact suppression measures, global stability, non-pharmaceutical interventions, respiratory syncytial virus, screen and isolation, sensitivity analysis

1 Introduction

Respiratory Syncytial Virus (RSV) which belongs to the genus Pneumoviridae is a significant contributor to respiratory infections. Several members of the RSV that belong to this genus include human RSV, bovine RSV and murine pneumonia virus. Based on the characterization of the G protein gene [the Glycoprotein (G) that facilitates attachment] [1], RSV in humans is divided into two major antigenic and genetic groups, namely RSV A and RSV B. The partial duplication of the G protein gene in RSV A (originally described

as the ON1 genotype) and RSV B (originally described as the BA genotype) is a notable feature of the strains currently circulating in the world population [2]. Understanding the distinction between these two strains is essential in the development of vaccines. While developing vaccines, determinants of early immune response to RSV need to be established [3]. This virus is prevalent worldwide and affects individuals of all age groups. We note however that the elderly, immunodeficient individuals, newborns, individuals with chronic obstructive lung disease and bronchial asthma are the most severely affected groups.

RSV associated with acute lower respiratory tract infection is the leading cause of mortality among respiratory infections. It is also the leading cause of hospitalization, and the second leading cause of death after malaria. According to the World Health Organization [4], RSV is associated with over 3.6 million hospitalizations and approximately 100 000 mortality cases in children under 5 years of age. A great majority of these pediatric RSV mortalities (about 97%) occur in low- and middle-income countries which are often characterized by inadequate Medicare support. Prematurity, being underweight at birth and the existence of co-morbid conditions like immunodeficiency, chronic respiratory disorders, and congenital heart disease, are additional risk factors. More still, living with older siblings, exposure to cigarette smoke, and lack of breastfeeding are additional factors that raise the risk of contracting RSV infection and its associated complications mostly among children.

In the review by [2] on the global distribution of RSV strains from the year 1961 to 2019, RSV A was the most common antigenic subgroup accounting for 60% of infections reported worldwide, 59.6% of infections reported in the Northern Hemisphere, and 61.9% of infections reported in the Southern Hemisphere. RSV B was only the predominant group worldwide, in nine seasons or years. For two or more consecutive seasons, this RSV group was not identified as predominant. However, when data were examined with respect to continents, it was found that there had been more RSV B infections than RSV A infections over the past decade, with RSV B predominating on all continents (except Asia) for several years in a row. Notably, RSV A and RSV B appeared to reach apparent equilibrium over the years at the conclusion of this analysis, which was associated with an increase in the overall prevalence of RSV B [2].

The major potential route of RSV transmission is via Respiratory droplets passing through the nasopharyngeal mucosa and into the upper respiratory tract (URT). Pneumonia, bronchiolitis, and other infections can arise from the preferential infection by syncytial virus of polarized ciliated epithelial cells of the human respiratory tract, which enter the lower respiratory tract (LRT) via the upper respiratory tract (URT) [5]. Upon infection with RSV, the lower respiratory tract is the most severely affected area of the respiratory system. The most typical symptoms include sneezing, coughing, wheezing, fever and loss of appetite [6]. For more details on the symptoms, interested readers may refer to [4, 7]. Research on the disease shows that a significant proportion of the population, around 40%, exhibit no symptoms [8]. This asymptomatic group may pose a significant problem in the disease transmission dynamics as super-spreaders.

Despite its significant impact, there is no approved RSV vaccine. However, while live attenuated vaccines are under development, they are primarily targeted at infants. More than 121 clinical trials have been conducted, but effective control remains challenging due to the high transmissibility of the virus. In addition, it is challenging to determine the exact prevalence of the disease given the fact that a significant proportion of the infected individuals do not show symptoms, the screening process can be costly, there is a possibility of misdiagnosis given the similarity of symptoms with other infections. More still, the absence of isolation protocols for infected individuals further complicates disease containment efforts. As a result, these complications or limitations can lead to under estimation of the RSV cases in the affected population. For this reason, the application of compartmentalized mathematical epidemic models could be beneficial. The compartmentalized and mechanistic models provide a clear explanation for the mechanisms of interaction between system components. In addition, specific biological theories are proposed to elucidate the dynamics of the infection including the influence of post-symptomatic infected individuals.

Several mathematical models have been proposed in literature to assess RSV epidemiology and interventions, and most of them are based on the SIR modeling framework. This is a compartmental model commonly used in epidemiology to describe the dynamics of infectious diseases within a population with the acronym SIR standing for Susceptible-Infectious-Recovered, indicating the three compartments that individuals in the population can be categorized into [9–11]. In the case where infected individuals recover with temporary immunity, the SIRS modeling framework is used. In the few paragraphs that follow, we provide some selected modeling studies on RSV.

Mathematical models have been used to estimate pediatric hospitalization costs and evaluate the cost-effectiveness of vaccination strategies. Notable RSV studies include: (1) The mathematical model in [12] which examined newborn vaccination strategies and their feasibility, (2) the model in [13] which assessed the impact of RSV in neonatal care. These mentioned models incorporated demographic factors, adult infection rates, and estimated key parameters such as birth and mortality rates, disease transmission rates, and hospitalization proportions. Acedo et al. [12] further refined these estimates using the Nelder-Mead algorithm, optimizing predictions to closely match observed hospitalization data for infants under one year of age in Valencia, Spain. Model validation was supported by consistent parameter values across different health districts.

Another key study by [14] analyzed seasonal RSV outbreaks and eradication thresholds. The study categorized the population into distinct groups (susceptible, infected, and immune) and employed deterministic ordinary differential equations (ODEs) to track disease progression. The analysis assumed equal birth and mortality rates, unit-scaled models, and fractions for state variables to simplify the analysis due to high annual infection rates. The model was used to explained patterns of regular yearly outbreaks and alternating large and small epidemic cycles. The findings of the study suggested that humidity influences RSV microbe survival

in experimental conditions, though its real-world impact remains uncertain.

A separate study by [15] analyzed pediatric RSV cases using demographic, clinical, and laboratory data, applying statistical tests such as the Student's *t*-test, ANOVA, chi-squared tests, and Fisher's exact test. The study highlighted the importance of understanding RSV interactions with other respiratory pathogens for effective case management, particularly in hospitalized patients. The results emphasize the importance of using epidemiological data to guide public health policies and vaccine development. The study notes some limitations which included uneven hospital distribution, low RSV detection rates due to antibiotic use, and the absence of viral load detection or RSV genotyping. These factors suggest that the findings may not fully capture the complete picture of RSV infection in pediatric patients in China from 2014–2018.

The main aims of this work include the following: (1) determining and quantifying the importance (significance) of the processes driving the transmission dynamics of the disease, (2) providing recommendations for public health officials, healthcare professionals, and policy-makers to use evidence-based strategies for RSV prevention and control of the disease, and (3) examine the effect of implementing pharmaceutical and non-pharmaceutical mitigation strategies on the timeliness of disease containment. This research also seeks to establish whether increased screening and recommendations for isolation would help in faster containment of the disease in case of an outbreak. We also seek to identify possible combinations of intervention measures that can lead to faster containment of the disease as well as lower burdens of the disease to the healthcare system.

The rest of the manuscript is organized as follows; In Section 2, a mathematical model for RSV is developed and analytical results are established. The model reproduction number is determined in Section 3 and the conditions for existence and stability of the disease-free equilibrium are established in the same section. In Section 4, the model endemic equilibrium is determined and its global stability established. Sensitivity analysis is performed in Section 5 to determine the most influential processes driving the disease dynamics. In Section 6, the model is numerically solved to determine the long-term behavior of the system and establish how different scenarios of mitigation measures affect the timeliness of disease containment. The manuscript is concluded in Section 7 where the findings of this study are summarized and further improvements to the models are suggested.

2 Model development and analysis

The total population is sub divided into 8 disjoint compartments where the individuals within a compartment are assumed to mix homogeneously and are indistinguishable with respect to the disease status. The compartments are as follows; the susceptible individuals (*S*) include all those at the risk of infection, exposed individuals (*E*), Symptomatic infected individuals (*I_s*), the asymptomatic infected individuals (*I_a*); asymptomatic individual may be identified through contact tracing (process is not explicitly modeled in the manuscript) and upon

screening are sent into isolation (*I_q*). The symptomatic individuals may develop severe disease and require admission into a hospital environment under the observation of healthcare workers. This class of individuals is denoted by *H*. The hospitalized individuals may be discharged upon management of the symptoms. We assume that some of these hospitalized individuals might have completely recovered while some might have not by the time they are discharged from hospital. The individual who might have been discharged hospital but still shedding the virus or are infectious are categorized as post-symptomatic individuals (*I_p*). The *I_p* class is considered owing to the fact that shedding can continue for at least 20 days after clinical recovery [16]. We further note that the post-symptomatic compartment can also be replenished by individuals who might have had symptoms in the early stages of the disease but were never detected or screened by the healthcare workers. This scenario is a common occurrence most especially when the symptoms are mild or treated as common cold or cough. The total population (*N*) is thus given by

$$N = S + E + I_a + I_s + I_q + H + I_p + R.$$

Note that the RSV transmission dynamics are similar to many other respiratory infections. In this manuscript, we use the force of infection that follows mass action incidence similar to that used in [12]. We note also that [12] in their force of infection proposed a contact term that captures seasonality exhibited by the RSV infection. This aspect was not explicitly modeled in our work owing to lack of RSV data. Since the body does not confer permanent immunity to RSV, individuals can contract the disease more than once in their life-time [17, 18]. The aspect that captures the waning of immunity is considered in the numerical simulations Section 6.3. The force of infection is given by

$$\lambda = \beta (I_a + \eta_1 I_s + \eta_2 I_p).$$

The terms η_1 and η_2 are transmission rates of individuals in the *I_s* and *I_p* classes relative to those in the *I_a* class. Since the individuals in the *I_s* class show symptoms, this will cause them to distance themselves from other individuals which in turn lowers their effective transmission rate. On the other hand, individual in the post-symptomatic class may mix more freely with the population but with a bit of precaution since they would have learned lessons from their ordeal with the disease. Intuitively, post-hospitalization individuals would be more cautious than those with mild symptoms who were never hospitalized coming from *I_s* class. Therefore, consideration of all post-symptomatic individuals in one class is as a simplifying assumption that could be refined in future work. Therefore, given these perceived interactions, we assume that the parameters η_1 and η_2 take on values such that $0 < \eta_2 < \eta_1 < 1$.

Based on the model assumptions, the schematic diagrams given in Figure 1 and the summary of state variables provided in Table 1, the resulting model describing the change in each state variable is

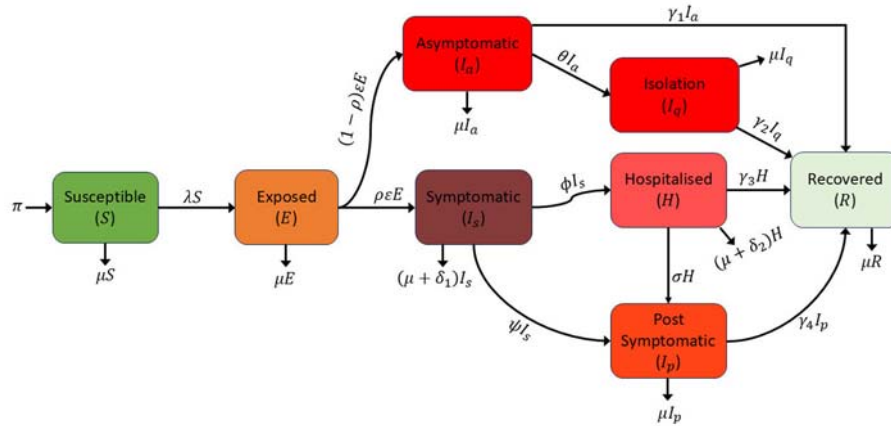


FIGURE 1 Schematic diagram showing the RSV disease progression and management strategies. The colors in the different state variables are indicative of perceived severity of the disease in compartments.

TABLE 1 Summary of model state variables and their descriptions.

State variable	Meaning
S	Susceptible individuals
E	Exposed individuals
I _a	Asymptomatic infected individuals
I _s	Symptomatic infected individuals
I _q	Screened and isolated asymptomatic individuals
H	Hospitalized individuals
I _p	Post-symptomatic infectious individuals
R	Recovered individuals

given in the system of Equation 1

$$\frac{dS}{dt} = \pi - \lambda S - \mu S, \tag{1a}$$

$$\frac{dE}{dt} = \lambda S - Q_1 E, \tag{1b}$$

$$\frac{dI_a}{dt} = (1 - \rho)\epsilon E - Q_2 I_a, \tag{1c}$$

$$\frac{dI_s}{dt} = \rho\epsilon E - Q_3 I_s, \tag{1d}$$

$$\frac{dI_q}{dt} = \theta I_a - Q_4 I_q, \tag{1e}$$

$$\frac{dH}{dt} = \phi I_s - Q_5 H, \tag{1f}$$

$$\frac{dI_p}{dt} = \sigma H + \psi I_s - Q_6 I_p, \tag{1g}$$

$$\frac{dR}{dt} = \gamma_1 I_a + \gamma_2 I_q + \gamma_3 H + \gamma_4 I_p - Q_7 R, \tag{1h}$$

where $Q_1 = (\mu + \epsilon)$, $Q_2 = (\mu + \theta + \gamma_1)$, $Q_3 = (\mu + \delta_1 + \phi + \psi)$, $Q_4 = (\mu + \gamma_2)$, $Q_5 = (\mu + \delta_2 + \sigma + \gamma_3)$, $Q_6 = (\mu + \gamma_4)$ and $Q_7 = \mu$.

The model has non-negative initial conditions given by

$$S(0) = S^0, E(0) = E^0, I_a(0) = I_a^0, I_s(0) = I_s^0, I_q(0) = I_q^0, H(0) = H^0, I_p(0) = I_p^0, R(0) = R^0.$$

2.1 Positive invariance of the domain Ω of biological significance

Owing to the fact that the model studies human populations, we ought to ensure that the population is non-negative and does not grow without bound. We therefore have the lemmas 1 and 2.

Lemma 1. *The solutions of the RSV model system (Equation 1) in the domain*

$$\Omega = \left\{ (S, E, I_a, I_s, I_q, H, I_p, R) \in \mathbb{R}_+^8 \mid S + E + I_a + I_s + I_q + H + I_p + R \leq \frac{\pi}{\mu} \right\}.$$

are non-negative for all $t > 0$.

Proof: The positivity of solutions of the model system (Equation 1) can be proved using various approaches including proof by contradiction [19], or based on the theory of differential inequalities [20, 21]. For this manuscript, we use the approach in the latter references. From the first equation of the model system (Equation 1), we have

$$\begin{aligned} \frac{dS}{dt} &= \pi + \omega R - \lambda S - \mu S, \\ &\geq -(\lambda(s) + \mu)S, \\ &\geq -(\hat{\lambda} + \mu)S, \text{ where } \hat{\lambda} = \max\{\lambda(s)\}. \end{aligned}$$

The obtained inequality can be solved by the method of separation of variables to obtain

$$S(t) \geq S^0 e^{-(\hat{\lambda} + \mu)t}.$$

Following the same approach, the rest of the state variables can be solved to obtain

$$\begin{cases} E(t) \geq E^0 e^{-Q_1 t}, \\ I_a(t) \geq I_a^0 e^{-Q_2 t}, \\ I_s(t) \geq I_s^0 e^{-Q_3 t}, \\ I_q(t) \geq I_q^0 e^{-Q_4 t}, \\ H(t) \geq H^0 e^{-Q_5 t}, \\ I_p(t) \geq I_p^0 e^{-Q_6 t}, \\ R(t) \geq R^0 e^{-Q_7 t}. \end{cases}$$

From the obtained results, we observe that all the state variables are non-negative for all $t \geq 0$. \square

Lemma 2. *The total population N for any initial values starting within the domain Ω is bounded, i.e., the population does not grow without bound.*

Proof: We observe that the total population (N) of the model (Equation 1) is not constant and the change in the total population is given by

$$\begin{aligned} \frac{dN}{dt} &= \pi - \mu N - \delta_1 I_s - \delta_2 H, \\ &\leq \pi - \mu N. \end{aligned}$$

The resulting equation can be solved using the integrating factor method to obtain

$$N(t) \leq \frac{\pi}{\mu} + \left(\frac{\pi}{\mu} - N_0 \right) e^{-\mu t},$$

which clearly indicates that the total population is bounded by $\frac{\pi}{\mu}$. We further note that for any initial population such that $0 < N(0) < \frac{\pi}{\mu}$, we have $0 < N(t) < \frac{\pi}{\mu}$ for all $t > 0$. Therefore, since the total population is bounded, then its sub-populations are also bounded. \square

Hence, the lemmas 1 and 2 indicate that the domain Ω is positively invariant. This implies that the solutions of the model system (Equation 1) with initial conditions starting in the domain Ω , also remain in the same domain.

3 Disease-free equilibrium and reproduction number

3.1 Disease-free equilibrium

The disease-free equilibrium (DFE) is evaluated by equating the right side of the model system (Equation 1) to zero and solving for the respective steady state values. At the DFE, there are no exposed nor infected individuals in the community. Therefore, the disease-free equilibrium for the respective state variables is given by

$$E_0 = \left(\frac{\pi}{\mu}, 0, 0, 0, 0, 0, 0 \right). \tag{2}$$

3.2 Model basic reproduction number

The reproduction number in the case of the RSV model studied in this work is the number of secondary infections generated in a purely susceptible community as a result of contact with an infected individual. Based on the force of infection given in Section 2, we note that there are three state variables (I_a , I_s , and I_p) contributing to new infections. Therefore, the reproduction number computed here should reflect the contribution of the aforementioned state variables. The model reproduction number is determined using the Next generation matrix method described in [22]. For ease of following the method used, we maintain the same notation for the matrix of new infections (\mathcal{F}) and the matrix of transitions (\mathcal{V}) between states used in [22]. For the model system of Equation 1, the matrices are given by

$$\mathcal{F} = \begin{bmatrix} \beta(I_a + \eta_1 I_s + \eta_2 I_p)S \\ 0 \\ 0 \\ 0 \\ 0 \\ 0 \\ 0 \end{bmatrix} \text{ and } \mathcal{V} = \begin{bmatrix} Q_1 E \\ -(1 - \rho)\varepsilon E + Q_2 I_a \\ -\rho\varepsilon E + Q_3 I_s \\ -\theta I_a + Q_4 I_q \\ -\phi I_s + Q_5 H \\ -\psi I_s - \sigma H + Q_6 I_p \end{bmatrix}.$$

The Jacobi of the matrices \mathcal{F} and \mathcal{V} evaluated at the disease free equilibrium give matrices \mathbf{F} and \mathbf{V} such that

$$\mathbf{F} = \begin{bmatrix} 0 & \beta \frac{\pi}{\mu} & \beta \eta_1 \frac{\pi}{\mu} & 0 & 0 & \beta \eta_2 \frac{\pi}{\mu} \\ 0 & 0 & 0 & 0 & 0 & 0 \\ 0 & 0 & 0 & 0 & 0 & 0 \\ 0 & 0 & 0 & 0 & 0 & 0 \\ 0 & 0 & 0 & 0 & 0 & 0 \\ 0 & 0 & 0 & 0 & 0 & 0 \end{bmatrix} \text{ and } \mathbf{V} = \begin{bmatrix} Q_1 & 0 & 0 & 0 & 0 & 0 \\ -(1 - \rho)\varepsilon & Q_2 & 0 & 0 & 0 & 0 \\ -\rho\varepsilon & 0 & Q_3 & 0 & 0 & 0 \\ 0 & -\theta & 0 & Q_4 & 0 & 0 \\ 0 & 0 & -\phi & 0 & Q_5 & 0 \\ 0 & 0 & -\psi & 0 & -\sigma & Q_6 \end{bmatrix}$$

respectively. Then the model basic reproduction number (\mathcal{R}_0) is given as the spectral radius (largest eigenvalue) of the matrix ($\mathbf{F} \cdot \mathbf{V}^{-1}$), in which case we have

$$\mathcal{R}_0 = \frac{\beta(1 - \rho)\varepsilon\pi}{\mu Q_1 Q_2} + \frac{\beta \eta_1 \rho \varepsilon \pi}{\mu Q_1 Q_3} + \frac{\beta \eta_2 \rho \varepsilon (\sigma \phi + \psi Q_5)}{\mu Q_1 Q_3 Q_5 Q_6}. \tag{3}$$

The three components $\mathcal{R}_{0I_a} = \frac{\beta(1 - \rho)\varepsilon\pi}{\mu Q_1 Q_2}$, $\mathcal{R}_{0I_s} = \frac{\beta \eta_1 \rho \varepsilon \pi}{\mu Q_1 Q_3}$ and $\mathcal{R}_{0I_p} = \frac{\beta \eta_2 \rho \varepsilon (\sigma \phi + \psi Q_5)}{\mu Q_1 Q_3 Q_5 Q_6}$ are the contributions of the infections classes I_a , I_s and I_p to the reproduction number and consequently to new infections. We note that the next-generation method in [22], presumes local stability of the disease-free equilibrium. Owing to this, we have the following lemma.

Lemma 3. *The disease-free equilibrium (Equation 2) of the RSV model (Equation 1) is locally asymptotically stable.*

Local asymptotic stability in Lemma 3 implies that if we start with initial states that are sufficiently close to the equilibrium (Equation 2), the trajectories of solutions converge to the equilibrium as times goes to infinity.

For readers interested in the proof of Lemma 3, they may consider linearising the model system (Equation 1) around the

equilibrium (Equation 2) and then evaluate the eigenvalues of the resulting Jacobian which will all be negative. We note that the negative eigenvalues of the resulting Jacobian matrix evaluated at the equilibrium point (Equation 2) indicate that the system of Equation 1 is asymptotically stable in the corresponding directions. This means that any perturbations around the equilibrium point, decay exponentially toward the equilibrium point as times goes to infinity.

3.3 Global stability of the disease-free equilibrium

The determination of global stability of the disease-free equilibrium of the model system (Equation 1) is aimed at confirming whether if we start at any point (not necessary nearby the equilibrium point but) within the domain, the trajectories of the system will approach the equilibrium point. We now pose the following theorem.

Theorem 1. *The disease-free equilibrium (\mathcal{E}_0) is globally asymptotically stable when $\mathcal{R}_0 < 1$ and unstable when $\mathcal{R}_0 > 1$.*

Proof: To prove the Theorem 1, we let

$$L = aE + bI_a + cI_s + dI_q + fH + gI_p$$

be a candidate Liapunov function, where a, b, c, d, f and g are nonnegative constants. We ought to find the constants a, b, c, d, f and g such that the derivative of the liapunov function is negative with respect to the associated state variable. The derivative of the Liapunov function is given by

$$\begin{aligned} \dot{L} &= a\dot{E} + b\dot{I}_a + c\dot{I}_s + d\dot{I}_q + f\dot{H} + g\dot{I}_p \\ &= a[\lambda S - Q_1E] + b[(1 - \rho)\varepsilon E - Q_2I_a] + c[\rho\varepsilon E - Q_3I_s] \\ &\quad + d[\theta I_a - Q_4I_q] + f[\phi I_s - Q_5H] + g[\sigma H + \psi I_s - Q_6I_p] \\ &\leq a[\beta(I_a + \eta_1 I_s + \eta_2 I_p)\frac{\pi}{\mu} - Q_1E] + b[(1 - \rho)\varepsilon E - Q_2I_a] \\ &\quad + c[\rho\varepsilon E - Q_3I_s] + d[\theta I_a - Q_4I_q] + f[\phi I_s - Q_5H] + g[\sigma H \\ &\quad + \psi I_s - Q_6I_p] \\ &= [-aQ_1 + b(1 - \rho)\varepsilon + c\rho\varepsilon]E + \left[a\beta\frac{\pi}{\mu} - bQ_2 + d\theta \right] I_a \\ &\quad + \left[a\beta\eta_1\frac{\pi}{\mu} - cQ_3 + f\phi + g\psi \right] \\ &\quad [-fQ_5 + \sigma g]H + \left[a\beta\eta_2\frac{\pi}{\mu} - gQ_6 \right] I_p - dQ_4I_q. \end{aligned}$$

Setting the coefficients of $E, I_a, H, I_p,$ and I_q to zero and solving for the constants, we obtain

$$\begin{cases} a = \mu Q_2 Q_6 \rho \varepsilon, \\ b = \beta \pi \rho \varepsilon Q_6, \\ c = Q_1 Q_2 Q_6 \mu - \beta \pi Q_6 (1 - \rho) \varepsilon, \\ d = 0, \\ f = \frac{\sigma \beta \eta_2 \pi Q_2 \rho \varepsilon}{Q_5}, \\ g = \beta \eta_2 \pi Q_2 \rho \varepsilon. \end{cases}$$

We the substitute the constants into the derivative of the Liapunov function to obtain

$$\begin{aligned} \dot{L} &\leq \left[\beta Q_3 Q_6 (1 - \rho) \varepsilon \pi + \beta \eta_1 \pi Q_2 Q_6 \rho \varepsilon + \frac{\beta \eta_2 \pi Q_2 \rho \varepsilon (\sigma \pi + \psi Q_5)}{Q_5} \right. \\ &\quad \left. - \mu Q_1 Q_2 Q_3 Q_6 \right] I_s = \mu Q_1 Q_2 Q_3 Q_6 (\mathcal{R}_0 - 1) I_s. \end{aligned}$$

It can be observed that the derivative of the Lyapunov function is negative when $\mathcal{R}_0 < 1$ and equality holds when $\mathcal{R}_0 = 1$ or when $I_s^* = 0$ which correspond to the disease-free equilibrium. Therefore, by the LaSalle invariance principle [23], the disease-free equilibrium \mathcal{E}_0 is globally asymptotically stable when $\mathcal{R}_0 < 1$ and unstable when $\mathcal{R}_0 > 1$. This completes the proof. \square

4 Existence of the endemic equilibrium and its stability

4.1 Existence of the endemic equilibrium

To determine the existence and uniqueness of the endemic equilibrium, we pose the following theorem.

Theorem 2. *Let \mathcal{E}_1 such that*

$$\mathcal{E}_1 = (S^*, E^*, I_a^*, I_s^*, I_q^*, H, I_p^*, R^*).$$

be the endemic equilibrium of the model system (Equation 1). The equilibrium \mathcal{E}_1 is unique and only exists when \mathcal{R}_0 is greater than unity.

Proof: To determine the endemic equilibrium, we set the left side of the model system (Equation 1) to zero to obtain the system (Equation 4), where the “*” indicates the value of the state variable at equilibrium

$$0 = \pi - \lambda^* S^* - \mu S^*, \tag{4a}$$

$$0 = \lambda^* S^* - Q_1 E^*, \tag{4b}$$

$$0 = (1 - \rho) \varepsilon E^* - Q_2 I_a^*, \tag{4c}$$

$$0 = \rho \varepsilon E^* - Q_3 I_s^*, \tag{4d}$$

$$0 = \theta I_a^* - Q_4 I_q^*, \tag{4e}$$

$$0 = \phi I_s^* - Q_5 H^*, \tag{4f}$$

$$0 = \sigma H^* + \psi I_s^* - Q_6 I_p^*, \tag{4g}$$

$$0 = \gamma_1 I_a^* + \gamma_2 I_q^* + \gamma_3 H^* + \gamma_4 I_p^* - Q_7 R^*. \tag{4h}$$

From the system of Equation 4, several equilibrium states can be expressed in terms of I_s^* to obtain

$$\begin{cases} E^* = \frac{Q_3 I_s^*}{\rho \epsilon}, \\ I_a^* = \frac{(1-\rho)Q_3}{\rho Q_2} I_s^*, \\ I_q^* = \frac{(1-\rho)\theta Q_3}{\rho Q_2 Q_4} I_s^*, \\ H^* = \frac{\phi}{Q_5} I_s^*, \\ I_p^* = \frac{(\sigma\phi + \psi Q_5)}{Q_5 Q_6} I_s^*, \\ R^* = \Phi I_s^*, \end{cases}$$

where $\Phi = \frac{\gamma_1(1-\rho)Q_3Q_4Q_5Q_6 + \gamma_2(1-\rho)\theta Q_3Q_5Q_6 + \gamma_3\phi q Q_2Q_4Q_6 + \gamma_4(\sigma\phi + \psi Q_5)\rho Q_2Q_4}{qQ_2Q_4Q_5Q_6Q_7}$. The term of the force infection at equilibrium is given by

$$\lambda^* = \frac{\beta [(1-\rho)Q_3Q_5Q_6 + \eta_1\rho Q_2Q_5Q_6 + \rho\eta_2(\sigma\phi + \psi Q_5)Q_2] I_s^*}{\rho Q_2Q_5Q_6}.$$

Substituting the appropriate terms into Equation 4 gives

$$\begin{aligned} & \frac{\beta [(1-\rho)Q_3Q_5Q_6 + \eta_1\rho Q_2Q_5Q_6 + \rho\eta_2(\sigma\phi + \psi Q_5)Q_2] I_s^* S^*}{\rho Q_2Q_5Q_6} \\ &= \frac{Q_1 Q_3}{\rho \epsilon} I_s^*. \end{aligned}$$

We note that one of the roots of this equation is $I_s^* = 0$, which solution corresponds to the disease free equilibrium. If $I_s^* \neq 0$, we simplify the expression further to obtain

$$\left[\frac{\beta(1-\rho)\epsilon}{Q_1 Q_2} + \frac{\beta\eta_1\epsilon\rho}{Q_1 Q_3} + \frac{\beta\eta_2\rho\epsilon(\sigma\phi + \psi Q_5)}{Q_1 Q_3 Q_5 Q_6} \right] S^* = 1,$$

which after multiplying both sides of the equation by $\frac{\pi}{\mu}$ gives

$$S^* = \frac{\pi/\mu}{\mathcal{R}_0}.$$

It is clear that the equilibrium value is unique and exists when $\mathcal{R}_0 > 1$. We further note that; substituting for λ^* , and S^* in Equation 4a we obtain the expression for I_s^* given by

$$I_s^* = \frac{\pi\rho\epsilon}{Q_1 Q_3} \frac{(\mathcal{R}_0 - 1)}{\mathcal{R}_0}.$$

such that $I_s^* > 0$ when $\mathcal{R}_0 > 1$. Consequently, the rest of the state variables at the steady state can be expressed in terms of \mathcal{R}_0 . Hence, the endemic equilibrium is unique and exists when $\mathcal{R}_0 > 1$. This completes the proof. \square

4.2 Global stability of the endemic equilibrium

In this section, we now prove the global stability of the RSV endemic equilibrium using a suitable Lyapunov function

Theorem 3. *The unique RSV equilibrium \mathcal{E}_1 is globally asymptotically stable when \mathcal{R}_0 is greater than unity.*

Proof: To prove the global stability of the equilibrium \mathcal{E}_1 , we propose a Liapunov function \mathcal{L} given by

$$\begin{aligned} \mathcal{L} = & (S - S^* - S^* \ln \frac{S}{S^*}) + (E - E^* - E^* \ln \frac{E}{E^*}) \\ & + (I_a - I_a^* - I_a^* \ln \frac{I_a}{I_a^*}) + (I_s - I_s^* - I_s^* \ln \frac{I_s}{I_s^*}) \\ & + (I_q - I_q^* - I_q^* \ln \frac{I_q}{I_q^*}) + (H - H^* - H^* \ln \frac{H}{H^*}) \\ & + (I_p - I_p^* - I_p^* \ln \frac{I_p}{I_p^*}) + (R - R^* - R^* \ln \frac{R}{R^*}). \end{aligned}$$

Using the approach outlined in [24], it can be shown that based on the constructed Liapunov function, the RSV persistent equilibrium states are the minimum points of the corresponding model state variables. The time derivative of the Liapunov function is given by

$$\begin{aligned} \frac{d\mathcal{L}}{dt} = & \left(1 - \frac{S^*}{S}\right) \frac{dS}{dt} + \left(1 - \frac{E^*}{E}\right) \frac{dE}{dt} + \left(1 - \frac{I_a^*}{I_a}\right) \frac{dI_a}{dt} \\ & + \left(1 - \frac{I_s^*}{I_s}\right) \frac{dI_s}{dt} + \left(1 - \frac{I_q^*}{I_q}\right) \frac{dI_q}{dt} + \left(1 - \frac{H^*}{H}\right) \frac{dH}{dt} \\ & + \left(1 - \frac{I_p^*}{I_p}\right) \frac{dI_p}{dt} + \left(1 - \frac{R^*}{R}\right) \frac{dR}{dt} \\ = & \left(1 - \frac{S^*}{S}\right) [\pi - \lambda S - \mu S] + \left(1 - \frac{E^*}{E}\right) [\lambda S - Q_1 E] \\ & + \left(1 - \frac{I_a^*}{I_a}\right) [(1-\rho)\epsilon E - Q_2 I_a] + \left(1 - \frac{I_s^*}{I_s}\right) [\rho\epsilon E - Q_3 I_s] \\ & + \left(1 - \frac{I_q^*}{I_q}\right) [\theta I_a - Q_4 I_q] + \left(1 - \frac{H^*}{H}\right) [\phi I_s - Q_5 H] \\ & + \left(1 - \frac{I_p^*}{I_p}\right) [\sigma H + \psi I_s - Q_6 I_p] \\ & + \left(1 - \frac{R^*}{R}\right) [\gamma_1 I_a + \gamma_2 I_q + \gamma_3 H + \gamma_4 I_p - Q_7 R]. \end{aligned}$$

We note that around the equilibrium point \mathcal{E}_1 , some constant terms can be expressed as

$$\begin{aligned} \pi = \lambda^* S^* + \mu S^*, \quad Q_1 = \frac{\lambda^* S^*}{E^*}, \quad Q_2 = \frac{(1-\rho)\epsilon E^*}{I_a^*}, \\ Q_3 = \frac{\rho\epsilon E^*}{I_s^*}, \quad Q_4 = \frac{\theta I_a^*}{I_q^*}, \quad Q_5 = \frac{\phi I_s^*}{H^*}, \\ Q_6 = \frac{\sigma H^* + \psi I_s^*}{I_p^*}, \quad Q_7 = \frac{\gamma_1 I_a^* + \gamma_2 I_q^* + \gamma_3 H^* + \gamma_4 I_p^*}{R^*}, \end{aligned}$$

which when substituted into the derivative of the Lyapunov function followed by appropriate factorisations of the resulting

expressions gives

$$\begin{aligned}
 \frac{d\mathcal{L}}{dt} = & \left(1 - \frac{S^*}{S}\right) \left[\mu S^* \left(1 - \frac{S}{S^*}\right) + \beta I_a^* S^* \left(1 - \frac{S}{S^*} \cdot \frac{I_a}{I_a^*}\right) \right. \\
 & + \beta \eta_1 I_s^* S^* \left(1 - \frac{S}{S^*} \cdot \frac{I_s}{I_s^*}\right) + \beta \eta_2 I_p^* S^* \left(1 - \frac{S}{S^*} \cdot \frac{I_p}{I_p^*}\right) \left. \right] \\
 & + \left(1 - \frac{E^*}{E}\right) \left[\beta I_a^* S^* \left(\frac{I_a S}{I_a^* S^*} - \frac{E}{E^*}\right) \right. \\
 & + \beta \eta_1 I_s^* S^* \left(\frac{I_s S}{I_s^* S^*} - \frac{E}{E^*}\right) + \beta \eta_2 I_p^* S^* \left(\frac{I_p S}{I_p^* S^*} - \frac{E}{E^*}\right) \left. \right] \\
 & + (1 - \rho) \varepsilon E^* \left(1 - \frac{I_a^*}{I_a}\right) \left[\frac{E}{E^*} - \frac{I_a}{I_a^*}\right] \\
 & + \rho \varepsilon E^* \left(1 - \frac{I_s^*}{I_s}\right) \left[\frac{E}{E^*} - \frac{I_s}{I_s^*}\right] + \theta I_a^* \left(1 - \frac{I_q^*}{I_q}\right) \left[\frac{I_a}{I_a^*} - \frac{I_q}{I_q^*}\right] \\
 & + \phi I_s^* \left(1 - \frac{H^*}{H}\right) \left[\frac{I_s}{I_s^*} - \frac{H}{H^*}\right] \\
 & + \left(1 - \frac{I_p^*}{I_p}\right) \left[\sigma H^* \left(\frac{H}{H^*} - \frac{I_p}{I_p^*}\right) + \psi I_s^* \left(\frac{I_s}{I_s^*} - \frac{I_p}{I_p^*}\right)\right] \\
 & + \left(1 - \frac{R^*}{R}\right) \left[\gamma_1 I_a^* \left(\frac{I_a^*}{I_a} - \frac{R^*}{R}\right) + \gamma_2 I_q^* \left(\frac{I_q^*}{I_q} - \frac{R^*}{R}\right) \right. \\
 & \left. + \gamma_3 H^* \left(\frac{H^*}{H} - \frac{R^*}{R}\right) + \gamma_4 I_p^* \left(\frac{I_p^*}{I_p} - \frac{R^*}{R}\right)\right]. \tag{5}
 \end{aligned}$$

Letting $F = \frac{S}{S^*}$, $G = \frac{E}{E^*}$, $U = \frac{I_a}{I_a^*}$, $V = \frac{I_s}{I_s^*}$, $W = \frac{I_q}{I_q^*}$, $X = \frac{H}{H^*}$, $Y = \frac{I_p}{I_p^*}$, $Z = \frac{R}{R^*}$, and then substituting the terms into the Equation 5 gives

$$\begin{aligned}
 \frac{d\mathcal{L}}{dt} = & \mu S^* \left(1 - \frac{1}{F}\right) (1 - F) + \beta I_a^* S^* \left(1 - \frac{1}{F}\right) (1 - FU) \\
 & + \beta \eta_1 I_s^* S^* \left(1 - \frac{1}{F}\right) (1 - FV) + \beta \eta_2 I_p^* S^* \left(1 - \frac{1}{F}\right) (1 - FY) \\
 & + \beta I_a^* S^* \left(1 - \frac{1}{G}\right) (FU - G) \\
 & + \beta \eta_1 I_s^* S^* \left(1 - \frac{1}{G}\right) (FV - G) + \beta \eta_2 I_p^* S^* \left(1 - \frac{1}{G}\right) (FY - G) \\
 & + (1 - \rho) \varepsilon E^* \left(1 - \frac{1}{U}\right) (G - U) \\
 & + \rho \varepsilon E^* \left(1 - \frac{1}{V}\right) (G - V) + \theta I_a^* \left(1 - \frac{1}{W}\right) (U - W) \\
 & + \phi I_s^* \left(1 - \frac{1}{X}\right) (V - X) \\
 & + \sigma H^* \left(1 - \frac{1}{Y}\right) (X - Y) + \psi I_p^* \left(1 - \frac{1}{Y}\right) (V - Y) \\
 & + \gamma_1 I_a^* \left(1 - \frac{1}{Z}\right) (U - Z) \\
 & + \gamma_2 I_s^* \left(1 - \frac{1}{Z}\right) (W - Z) + \gamma_3 H^* \left(1 - \frac{1}{Z}\right) (X - Z) \\
 & + \gamma_4 I_p^* \left(1 - \frac{1}{Z}\right) (Y - Z).
 \end{aligned}$$

We use the inequality $v(x) = 1 - x + \ln x < 0$ for all $x > 0$, in which case $1 - x < -\ln x$ to determine the signs of the components

of the derivative of the Lyapunov function. To show that all terms are negative, we demonstrate this with the a selection of terms, for example

$$\begin{aligned}
 \left(1 - \frac{1}{F}\right) (1 - FU) &= 1 - \frac{1}{F} - FU + U \\
 &\leq -\ln \frac{1}{F} - FU + U \\
 &\leq -\ln \frac{1}{F} + 1 - FU - 1(1 - U) \\
 &\leq -\ln \frac{1}{F} - \ln(FU) + \ln(U) \\
 &= -\ln(U) + \ln(U) \\
 &= 0.
 \end{aligned}$$

We also observe that the term $\left(1 - \frac{1}{F}\right) (1 - F) = -\frac{1}{F}(1 - F)^2$. Using the same inequality $1 - x < -\ln x$, it can be shown that the rest of the terms (i.e the product terms in brackets) of the Lyapunov derivative are also less than zero. Therefore, $\frac{d\mathcal{L}}{dt} \leq 0$ when $\mathcal{R}_0 > 1$ and equality holds at the steady state in which case $F = G = U = V = W = X = Y = Z = 1$. Thus, by the LaSalle invariance principle [23], when $\mathcal{R}_0 > 1$, the solutions of the model system (Equation 1) approach the endemic equilibrium as t grows very large. The above observation confirms that the endemic equilibrium \mathcal{E}_1 is globally asymptotically stable. \square

5 Numerical simulations

5.1 Parameter estimation

In this section, we estimate the model parameters mostly from biological studies and, published literature. The time-line from exposure to the disease to recovery is summarized in [25]. The effective contact rate (β) of the disease depends on the number of contacts a susceptible individual makes with infectious individuals as well as the probability that a contact is likely to result into disease transmission. In addition, the infectious dose of RSV is more than 160 – 640 viral units [16] and the risk of infection varies with different age groups. Therefore, the value of β can vary considerably depending on the studies conducted, even with estimations from different data sources. The values of the relative transmission rates η_1 and η are assumed bearing in mind the assumption given in Section 2. We further note that, shedding of RSV can continue for over 20 days after clinical recovery [16]. There are different transition rates into the post-symptomatic compartment from the symptomatic and hospitalized classes depending on the health of individuals. The transition from the asymptomatic class (I_a) to the isolated class (I_q) is achieved through contact tracing and screening of the identified individuals who test positive for the disease. This transition rate is influenced by several factors that determine the effectiveness of the contact tracing process. Some of the influential factors include, the size of the outbreak, perceived benefit and utilization of the process, effectiveness of the surveillance process and technology, and community engagement among others. The description of the model parameters, the selected ranges of the values of the parameters and corresponding nominal values are presented in Table 2.

TABLE 2 Description of parameters and estimation of nominal values.

Parameter	Description	Range	Nominal value	Source
π	Recruitment rate		$\mu \times N_0$	Assumed
β	Effective contact rate		$4.6 \times 10^{-6} \text{ day}^{-1} \text{ person}^{-1}$	Assumed
η_1	Transmission by I_s relative to I_a		0.68 day^{-1}	Assumed
η_2	Transmission by I_s relative to I_p		0.425 day^{-1}	Assumed
ε	Progression rate from E to infectiousness	$(\frac{1}{8}, \frac{1}{2})$	$1/6 \text{ day}^{-1}$	[25]
ρ	Proportion of the infected who are symptomatic		0.4	[29]
μ	Natural death rate		$1/(365 \times 60) \text{ day}^{-1}$	[30]
θ	Screening and isolation rate of I_a to I_q		0.02 day^{-1}	Assumed
ϕ	Screening and rate admission of I_s to H		0.5 day^{-1}	Assumed
ψ	Progression rate from I_s to I_p		0.058 day^{-1}	Assumed
σ	Transfer rate from the Hospitalization to post-symptomatic stage		0.142	Assumed
δ_1	Disease induced death rate of I_s		0.21 day^{-1}	[31]
δ_2	Disease induced death rate of H		0.05 day^{-1}	[31]
γ_1	Recovery rate of I_a	$(\frac{1}{14}, \frac{1}{7})$	1/14	[6, 25]
γ_2	Recovery rate of I_q	$(\frac{1}{14}, \frac{1}{7})$	1/10	[6, 25]
γ_3	Recovery rate of H	$(\frac{1}{14}, \frac{1}{7})$	1/12	[6, 25]
γ_4	Recovery rate of I_p	$(\frac{1}{14}, \frac{1}{7})$	1/16	[6, 25]
ω	Waning rate of immunity	$(\frac{1}{365}, \frac{1}{90})$	1/60	[17]

5.2 Sensitivity analysis of the model parameters

Given the uncertainty in estimation of model parameters for published literature, it is essential to perform sensitivity analysis to ascertain how different process affect the disease dynamics. When performing sensitivity analysis, variations are made in the input parameter values and the resulting measured output can be used to determine the processes to be targeted if the infection is to be contained. Sensitivity analysis approaches can be categorized into two, namely; local (where one parameter is varied at a time while keeping the others constant), or global (where several parameters values can be varied simultaneously) [9]. Several approaches some of which are listed in [20] have been used to perform sensitivity analysis with respect to different problems. In this paper, we use the Latin hypercube sampling (LHS) scheme [26] which is a stratified sampling method that allows for simultaneous sampling of the a multi-dimensional parameter space. The LHS method was first applied in epidemiological models, particularly with an HIV model as an example in [26]. The LHS being a stratified method, independent of dimension, it is a suitable approach for global sensitivity analysis of epidemiological models. In this manuscript, we follow the approach detailed in [27] for which 1,000 simulations were done for each run and the parameter specific partial rank correlation coefficients (PRCCs) were determined. Here, we considered two case, namely (1) sampling selected parameters including variable contact rate, and (2) sampling selected parameters in the reproduction number when the contact rate is assumed to be constant. This two step procedure is aimed at ascertaining whether the significance of the effective contact rate may potentially confound the influence of other parameters.

5.2.1 Sensitivity analysis of \mathcal{R}_0 when the contact rate is variable

The results of the PRCCs for the sampled parameter space are given in the Tornado plot (Figure 2a) and the box plot (Figure 2b) details the variability of the values of the reproduction number computed from the sampling procedure.

The tornado plot (Figure 2a) shows that the only significantly sensitive parameter is β which represents the effective contact rate. The five number summary of the values of the reproduction number calculated from the sampling procedure are such that; minimum = 0.35, lower Quartile (Q_1) = 0.73, median = 1.12, upper quartile (Q_3) = 1.50, and the maximum = 1.91. From the five number summary displayed in Figure 2b, we obtain an interquartile range of 0.77. This measure of spread of the middle distribution of the computed values of the reproduction number can be quite significant in disease dynamics most especially in big populations. The values of \mathcal{R}_0 displayed in Figure 2b indicate that there are combinations of processes described by the sampled parameters for which the disease can either be contained or made worse. For the sampled parameter space, p -values of the respective PRCCs are computed using the approach detailed in [26, 27] and the results are summarized in Table 3.

Based on the results in Figure 2a and Table 3, it is evident that enhancing preventive measures such as practicing regular hand hygiene, which includes washing your hands with clean water and soap, or using hand sanitizer can help contain the spread of the disease [28]. Additional advise to individuals is to cover coughs and sneezes with their elbow instead of the hands, wearing a respirator or face mask most especially in crowded places [28].

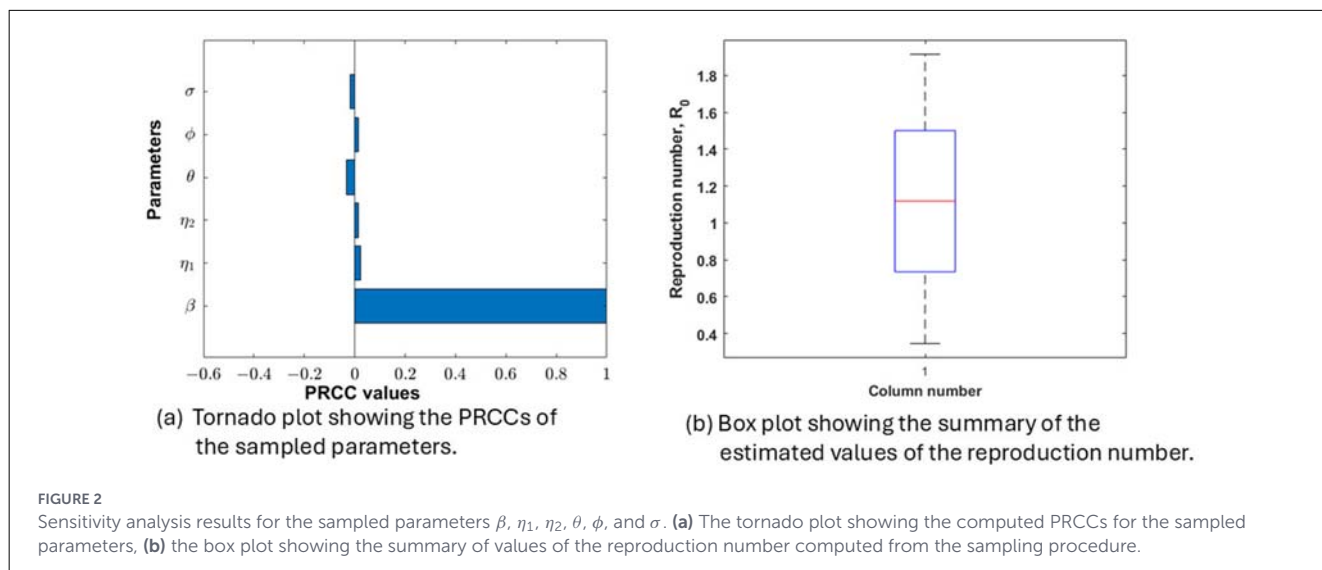


FIGURE 2

Sensitivity analysis results for the sampled parameters β , η_1 , η_2 , θ , ϕ , and σ . (a) The tornado plot showing the computed PRCCs for the sampled parameters, (b) the box plot showing the summary of values of the reproduction number computed from the sampling procedure.

TABLE 3 Summary of the PRCCs and corresponding p-values for the sampled parameters.

Parameter	Parameter range	Nominal value	PRCC	FDR adjusted p-value	Significant
β	$(1.2 \times 10^{-6}, 6.5 \times 10^{-6})$	4.2×10^{-6}	0.9994	0.000	Yes
η_1	(0.0412, 0.0648)	0.058	0.0440	0.3311	No
η_2	(0.03825, 0.041)	0.039	0.0318	0.4746	No
θ	(0.018, 0.022)	0.02	-0.0521	0.3015	No
ϕ	(0.45, 0.55)	0.5	0.0240	0.5395	No
σ	(0.02385, 0.02915)	0.0265	-0.0050	0.8749	No

5.2.2 Sensitivity analysis of \mathcal{R}_0 when the contact rate is constant

The sensitivity analysis considered here is aimed at ascertaining whether the significant influence of contact rate on the reproduction number may have confounding effect on any of the parameters that are initially viewed not to be significantly sensitive. For the sensitivity analysis case considered in this part, we assume that the effective contact rate is maintained at the baseline value similar to all the other parameters which are not listed in Table 4.

The tornado plot, Figure 3a shows that the significantly sensitive parameter is θ which represents the screening and isolation of infected individuals. Since the parameter has a negative PRCC, it indicates that increasing the screening and isolation rate of infected individuals helps reduce the likelihood of infection. The five number summary of the values of the reproduction number calculated from the sampling procedure are such that; minimum = 1.195, lower Quartile (Q_1) = 1.209, median = 1.221, upper quartile (Q_3) = 1.235, and the maximum = 1.250 (see Figure 3b). The computed values of reproduction number have an interquartile range (IQR) of 0.026, which shows a very narrow spread of the middle half of the distribution of the computed values of the reproduction number.

5.2.3 Pairwise comparison of selected processes

We compare the relative influence of the changes in the effective contact rate (β) and (1) screen and isolation, (2) transfer rate of individuals from the hospital to the post-symptomatic stage. The consideration for screening and isolation is to draw insights from the results on whether it may be justified to recommend for such processes to be implemented in case of an outbreak. Our analysis showed that when both contact rate and screening parameters are varied, only the contact rate significantly affects the reproduction number-highlighting its dominant role in transmission dynamics. The results of the pairwise comparison of control parameters are given in Figure 4.

We note from Figure 4a that, keeping the screening rates (θ) constant, a 23% $\left(\frac{(5.2-4) \times 10^{-6}}{5.2 \times 10^{-6}} \times 100\right)$ decrease in the effective contact rate (β), results in a reduction of approximately 25% $\left(\frac{1.6-1.2}{1.6} \times 100\right)$ in the reproduction number. Conversely, when the contact rate is held constant, increasing the screening and isolation rate by (θ) by 44.4% $\left(\frac{0.026-0.018}{0.018} \times 100\right)$ results in only a modest 7% $\left(\frac{1.4-1.3}{1.4} \times 100\right)$ reduction of the reproduction number which suggests diminishing returns for this strategy. This observation raises pertinent questions on whether a recommendation for widespread screening and isolation during a RSV outbreak would be justified. We note however that, the importance of any intervention measure that saves lives can not

TABLE 4 Summary of the PRCCs and corresponding p-values for the sampled parameters.

Parameter	Parameter range	Nominal value	PRCC	FDR adjusted p-value	Significant
η_1	(0.0412, 0.0648)	0.058	0.0517	0.2574267	No
η_2	(0.03825, 0.041)	0.039	0.0144	0.6499708	No
θ	(0.018, 0.022)	0.02	-0.9985	0.0000000	Yes
ϕ	(0.45, 0.55)	0.5	-0.04510	0.2583038	No
σ	(0.02385, 0.02915)	0.0265	-0.0200	0.6499708	No

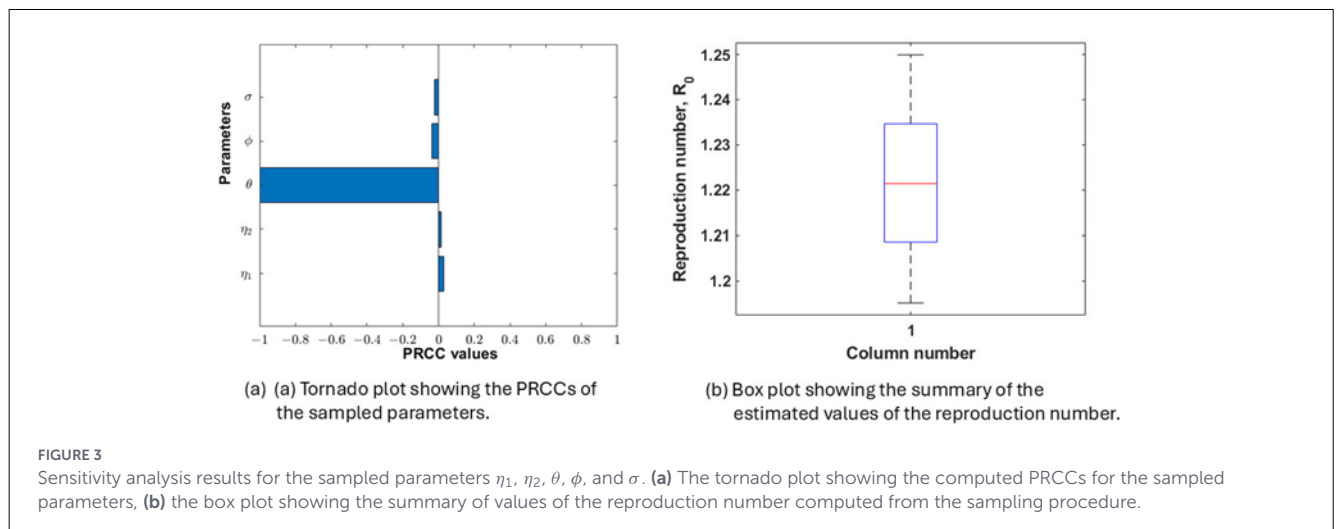


FIGURE 3 Sensitivity analysis results for the sampled parameters η_1 , η_2 , θ , ϕ , and σ . (a) The tornado plot showing the computed PRCCs for the sampled parameters, (b) the box plot showing the summary of values of the reproduction number computed from the sampling procedure.

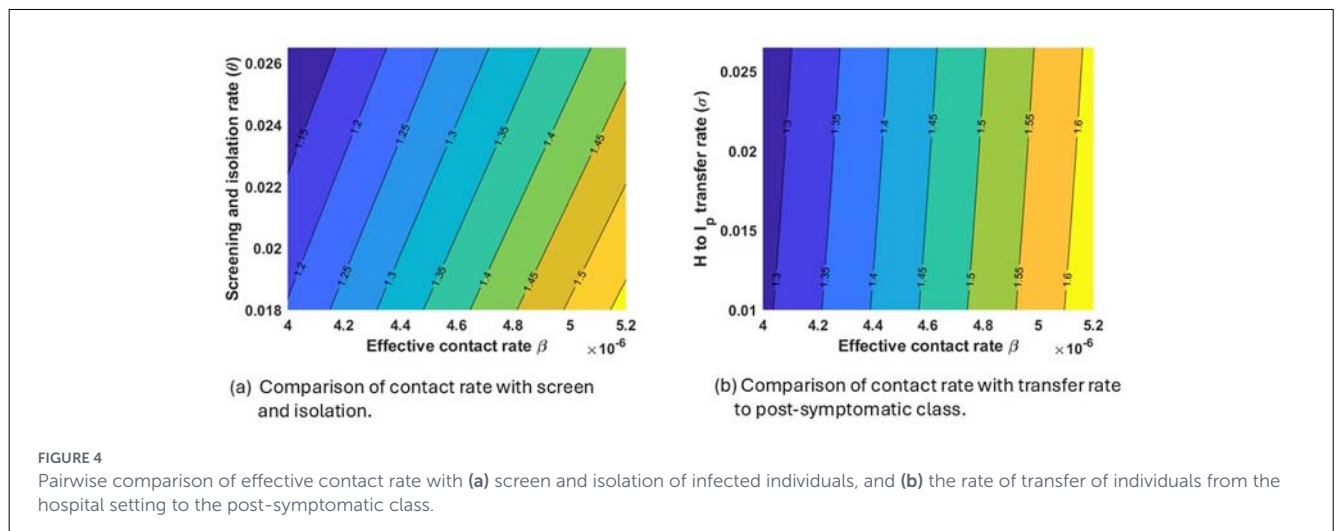
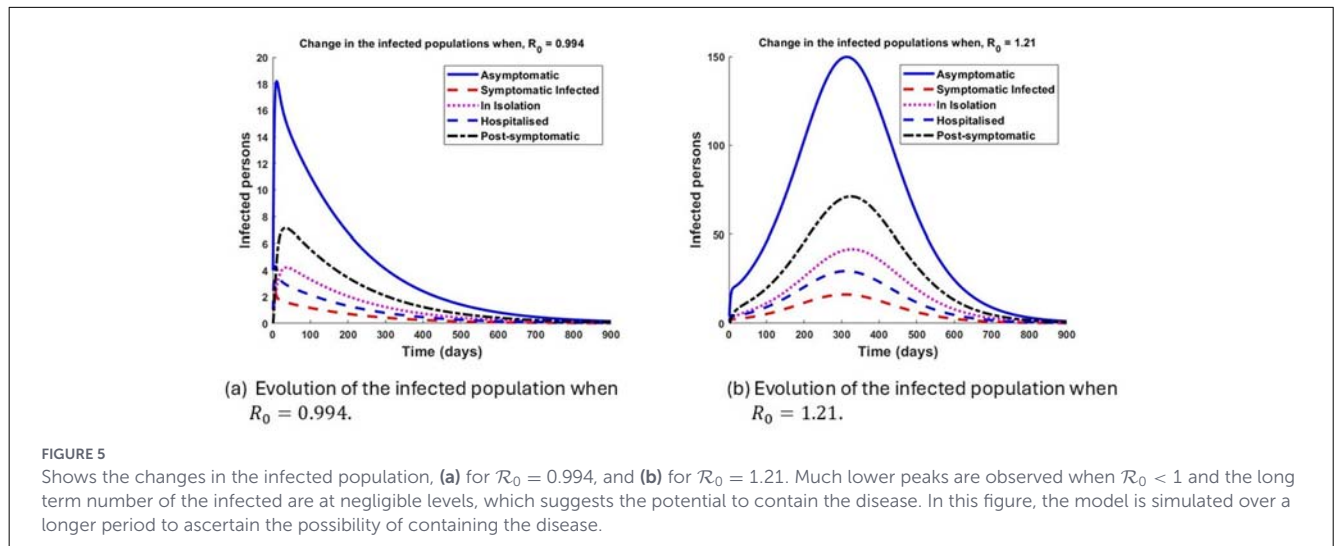


FIGURE 4 Pairwise comparison of effective contact rate with (a) screen and isolation of infected individuals, and (b) the rate of transfer of individuals from the hospital setting to the post-symptomatic class.

be over emphasized. In addition, in cases of large outbreaks, even a 7% reduction in the reproduction number can save many lives. In Figure 4b, when the transfer rate from the hospitalized class to the post-symptomatic class is kept constant, we observe a 19% reduction in the reproduction number for a 23% reduction in effective contact rate. On the other hand, a change in the transfer rate from hospitals to the post-symptomatic class results in a negligible reduction in the reproduction number. The results obtained in the pairwise comparison of the considered controls emphasize the need to focus on preventive measures indicated in Section 5.2.1 if the disease is to be contained.

6 Numerical results

We implemented the numerical simulations of the model using the fourth-order Runge-Kutta method *ODE45* in Matlab R2023b. The parameter values used in the simulations are detailed in Table 2. We used the numerical simulations to determine the long term dynamics of the system, for the initial values $(S^0, E^0, I_a^0, I_s^0, I_q^0, H^0, I_p^0, R^0)$ respectively given as $(50,000, 50, 4, 1, 1, 1, 0, 0)$. The recruitment rate is given by $\mu \times N_0$ where N_0 is the total initial population.



6.1 Conditions for existence and containment of the infection

The model system of Equation 1 was simulated for a selected set of parameters for which the reproduction number is either greater than or below 1. The results are presented in Figure 5.

The results show an initial increase in the infected population followed by a decline. This decline is attributed to self-limitation of the disease resulting from depletion of the susceptible population which consequently reduces the probability of new infections. The obtained results predict that the disease can be contained in the long term if intervention measures are put in place that reduce the reproduction number below 1. The results in Figure 5 show negligible long-term numbers of infected individuals.

6.2 Scenarios of mitigation measures with no waning immunity

6.2.1 Implementation of contact suppression measures

The epidemiology of the disease can be managed by implementing disease contact suppression mechanisms. Here, we consider two scenarios; (1) a case when the suppression mechanisms are implemented right at the beginning of the outbreak, or when the disease cases are detected, and (2) when the mitigation strategies are implemented later on during the course of the disease. We seek to ascertain how each of the strategies impacts on the model reproduction number, the peak values of the infection and the expected time during the outbreak when the peaks can be reached. These scenarios help in informing policy makers on the best course of action when implementing this strategy. In our simulation approach, the baseline contact rate is the value indicated in Table 2. We then consider new contact rates $\beta(1 - \alpha)$, where α accounts for the percentage reduction. In this case, we considered reductions of 20%, 40% and 60% from the baseline value as possible scenarios.

We implemented the changes and simulated the model system to determine the long term behavior of each of the state variables.

The results for the changes in the population of asymptomatic and symptomatic infected individuals as representative cases are indicated in Figure 6.

The values of peak values of the asymptomatic individuals computed for different scenarios of contact suppression measures are used to give a general indication of the trends of the sub-populations. The summary of the peak values, the times at which the peaks are attained, the computed values of the reproduction number and their corresponding percentage changes, as well as percentage changes in the peak asymptomatic cases are presented in Table 5.

It can be observed that the change in the values of R_0 is inversely proportion to percentage change in contact suppression measures. On the other hand, the peak values decrease exponentially with the increase in contact suppression measures.

6.2.2 Comparison between early and late implementation of contact suppression measures

We compare the scenarios when the contact suppression measures are either implemented in the very early stages of the outbreak or slightly later on as the disease progresses. Here, we used the variation in the hospitalized population as a representation of the changes occurring in different state variables. The procedure followed when implementing the changes in contact rate (β) are as described in Section 6.2.1. The results are presented in Figure 7.

We observe that when contact suppression strategies are implemented in the early stages of the outbreak, it results in lower peak values of the individuals requiring hospitalization and peaks are attained at later time when compared to a scenario where the implementation of mitigation measures is delayed.

6.2.3 Implementation of stringent screening and isolation measures

We considered variations from the baseline isolation rate using the expression $\theta(1 + \alpha)$, a scenario which depicts tightening of infection control programs directed toward mitigation measures

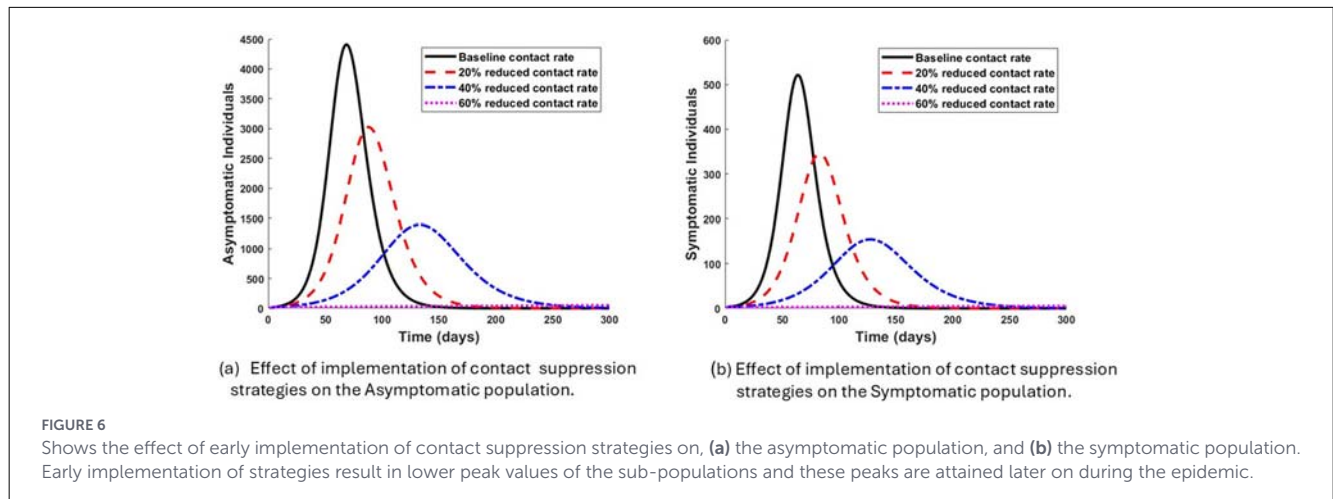


TABLE 5 Changes in the reproduction number and peak values of the asymptomatic individuals for different levels of contact suppression measures.

Time position of the main peak	69	88	133	300
Main peak value of asymptomatic individuals	4,410	3,025	1398	50
%age change in the main peak values from the baseline	—	-31.4	-68.3	98.9
Computed values of \mathcal{R}_0	2.98	2.39	1.79	1.19
%age change in \mathcal{R}_0 from the baseline	—	-20	-40	-60

such as contact tracing, screening and isolation of asymptomatic infected individuals. The numerical results for the two significantly changing compartments are given in Figure 8.

With the implementation of screening and isolation, considerable differences in the changes in populations were observed for the asymptomatic and isolated individuals. The main peak values for the asymptomatic class were observed at around 55–56 days (see Figure 8a) while the peaks were observed at around 75–76 days for the individual in isolation (see Figure 8b). The rest of the compartments did not show significant changes in either the peak or equilibrium values. It is clear that there are more pronounced differences in the peak values for the compartment of individuals in isolation (see Figure 8b) compared to the compartment of asymptomatic individuals (see Figure 8a).

6.3 Effect of waning immunity on the disease dynamics

Exploration of the effect of immunity on the disease dynamics was done by simulating the model for the case when immunity does not wane during the modeling time, and a case when recovered individuals remain immune for only 6 months after which immunity wanes. It should be noted that, waning of immunity contributes to replenishment of the susceptible population. The model system of Equation 1 was adjusted to include a loop from the

recovered class to the susceptible class to obtain updated system of Equation 6.

$$\begin{aligned} \frac{dS}{dt} &= \pi + \omega R - \lambda S - \mu S, \\ &\vdots \\ \frac{dR}{dt} &= \gamma_1 I_a + \gamma_2 I_q + \gamma_3 H + \gamma_4 I_p - (\mu + \omega)R. \end{aligned} \tag{6}$$

Note that only the equations for the susceptible and recovered individuals are changed. The two considered cases are indicated in Figure 9a (a case with waning immunity), and Figure 9b, a case when immunity does not wane within the modeling time. In both aspects, the reproduction number is greater than unity.

The model predicts recurrent waves of the disease when immunity doesn't last long. On the contrary, only one major outbreak is predicted and the disease wouldn't be sustained when the population has prolonged immunity to the disease. In particular, if mitigation measures that boost or prolong immunity to RSV are implemented, the disease can be contained since there won't be enough replenishment of the susceptible population to sustain the epidemic.

6.3.1 Implementation of stringent screening and isolation measures when $\omega \neq 0$

The model system of Equation 6 was simulated using the approach described in Sections 6.2.3. In particular, variations were made to the baseline isolation rate using the expression $\theta(1 + \alpha)$. We note that the adjusted model system (Equation 6) accounts for replenishment of the susceptible population from recovered individuals whose immunity has waned. The numerical results for the two significantly changing compartments are given in Figure 10.

More specifically, the changes in the number of asymptomatic individuals is presented in Figure 10a and the individuals in isolation are presented in Figure 10b. It can be observed that an increase in the screening and isolation rates results in the depletion of the asymptomatic population and replenishment of the isolated population. Significant changes for the two considered

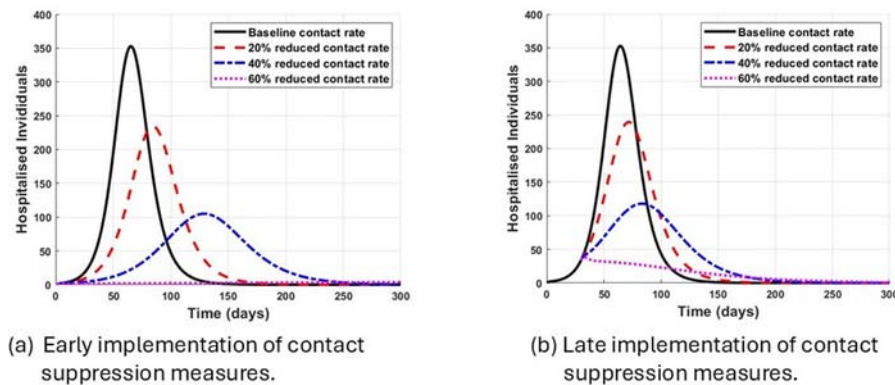


FIGURE 7 Shows the effect of (a) early implementation of contact suppression strategies, (b) late implementation of contact suppression strategies on the hospitalized population. Early implementation of strategies result in lower peak values of hospitalisations.

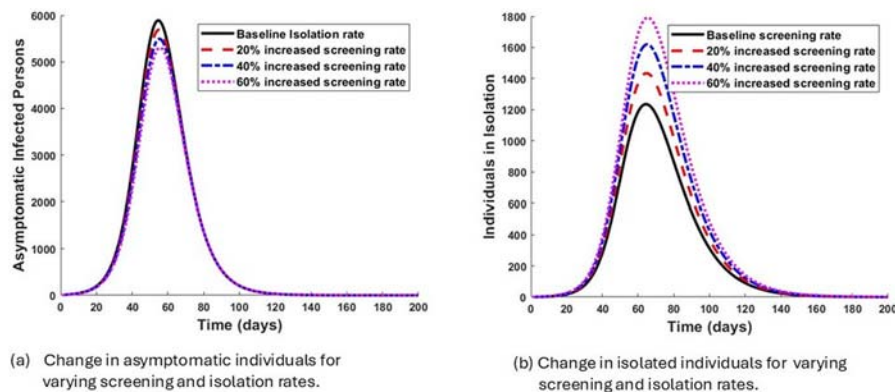


FIGURE 8 Shows the change in (a) asymptomatic individuals, (b) isolated individuals for varying values of isolation rates.

compartments are observed around the peak positions. In Table 6, we present the changes in the reproduction number and peak values of the asymptomatic individuals for different rates of screening and isolation.

The trend and percentage changes for the isolated population differ slightly from those of the asymptomatic class as observed in Figure 10 where an increasing in screening rate resulted in the replenishment of the isolated population hence the positive values for the changes in peak values from the baseline (see Figure 10b).

6.3.2 Contact suppression measures in presence of waning immunity

We implemented the changes in the contact rate (using the same approach indicated in Section 6.2.1) and simulated the model system (Equation 6) to determine the long term behavior of each of the state variables. The results for the changes in the population of asymptomatic and symptomatic infected individuals as representative state variables are indicated in Figure 11.

The simulation results predict that the infection would result in at least two waves of the epidemic with the second wave

less severe than the first. In all cases, the scenario with higher implementation of contact suppression strategies is characterized by lower peaks of the number of infected. We observe that with up to 40% increase in contact suppression measures, the disease dynamics exhibit only one wave, and with at least a 60% increase from the baseline value, the disease may be contained. This scenarios is observed even when the model simulation is run for a much longer time, where negligible numbers of infected individuals are predicted. We then compare the scenarios when the disease mitigation measures are either implemented in the very early stages of the outbreak or slightly later on as the disease progresses. Here, we used the variation in the hospitalized population as a representation of the changes occurring in different state variables. The results are presented in Figure 12.

We observe that when contact suppression strategies are implemented in the early stages of the outbreak, it results in lower and later peak values of the individuals requiring hospitalization. When the implementation of mitigation measures is delayed, higher and earlier peaks of the infected are observed when compared to the where control measures are applied early in the outbreak.

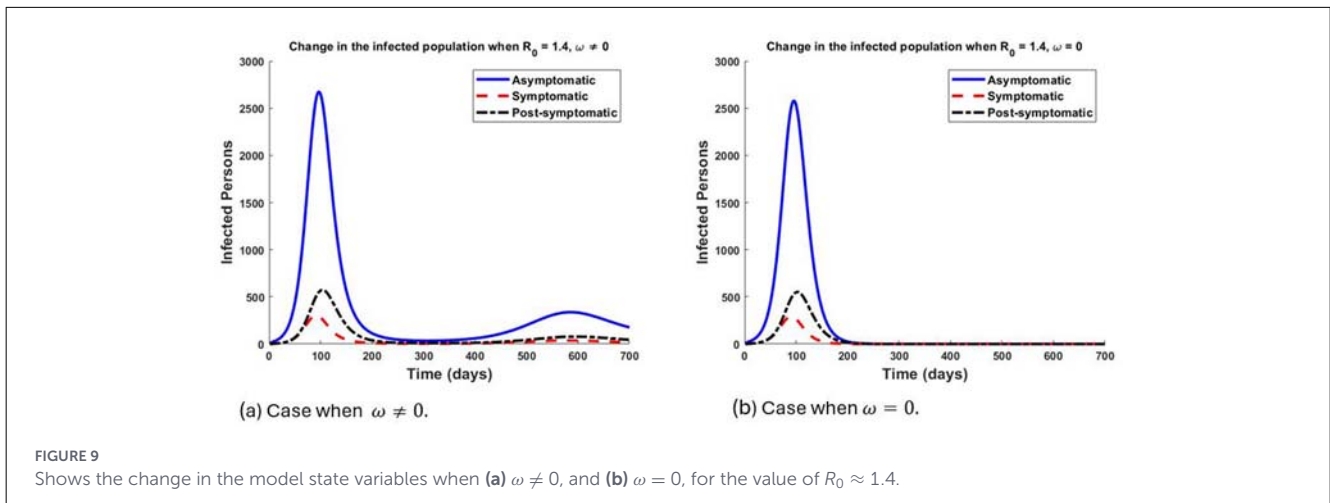


FIGURE 9 Shows the change in the model state variables when (a) $\omega \neq 0$, and (b) $\omega = 0$, for the value of $R_0 \approx 1.4$.

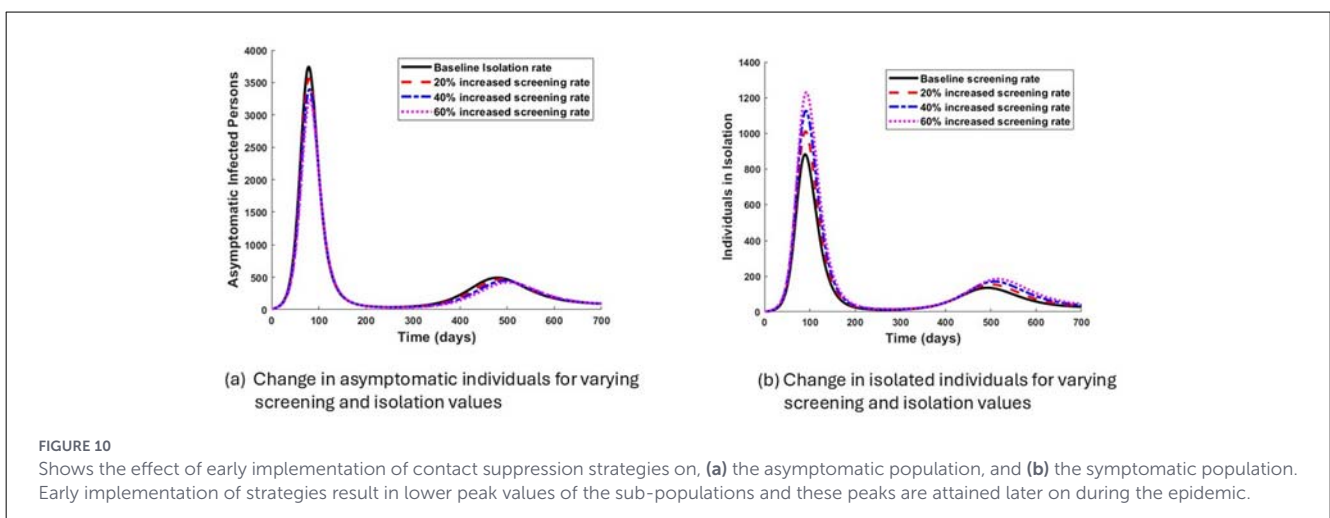


FIGURE 10 Shows the effect of early implementation of contact suppression strategies on, (a) the asymptomatic population, and (b) the symptomatic population. Early implementation of strategies result in lower peak values of the sub-populations and these peaks are attained later on during the epidemic.

7 Discussion and conclusion

A mathematical model describing the transmission dynamics of Respiratory Syncytial virus was developed and used to explore different scenarios under which the disease can be contained. The population considered was classified into 8 disjoint compartments but the individuals in each compartment were assumed to mix homogeneously. Basic properties of the model were determined including, positivity and boundedness of solutions, the model basic reproduction number, as well as the equilibrium points. The basic model has a disease free equilibrium which exists when the reproduction number is below 1 and is globally stable. In addition, a unique endemic equilibrium exists when the reproduction number is greater than one and it is globally stable. Global sensitivity analysis of selected model parameters as input values and the values of the reproduction number as the output was performed. The results indicated that increased contact between the susceptible and infectious individuals has the greatest potential of making the epidemic worse. It was also observed that including the contact rate in the sensitivity analysis computations may have a confounding effect on other processes that influence the disease dynamics. For example, it was observed that when the contact

TABLE 6 Changes in the reproduction number and peak values of the asymptomatic individuals for different levels of screening and isolation.

Time position of the main peak	79	79	80	81
Main peak value of asymptomatic individuals	3,743	3,564	3,395	3,234
%age change in the main peak values from the baseline	—	-4.78	-9.30	-13.60
Computed values of \mathcal{R}_0	1.55	1.51	1.48	1.45
%age change in \mathcal{R}_0 from the baseline	—	-2.58	-4.52	-6.45

rate is kept constant, the sensitivity analysis results showed that isolation practices can play a significant role in containing the disease.

Numerical simulations were performed to explore the long-term behavior of the model. The results predicted that the disease remains persistent when the reproduction is greater than one and can be contained when the reproduction number is reduced to below one. Different scenarios of intervention

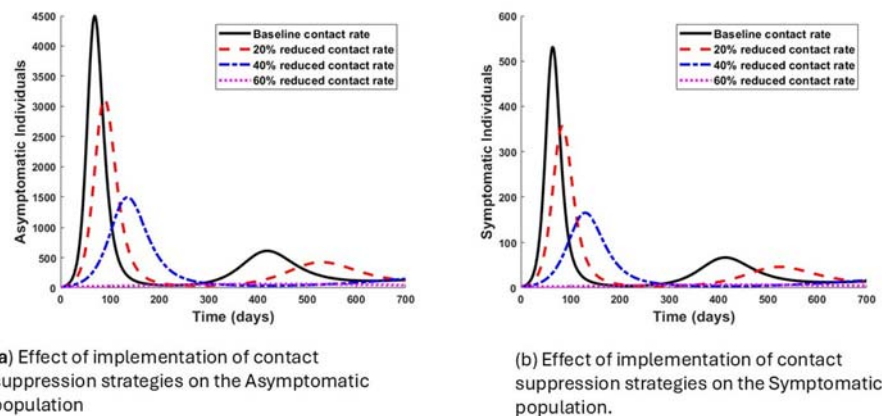


FIGURE 11

Shows the effect of early implementation of contact suppression strategies on, (a) the asymptomatic population, and (b) the symptomatic population. Early implementation of strategies result in lower peak values of the sub-populations and these peaks are attained later on during the epidemic.

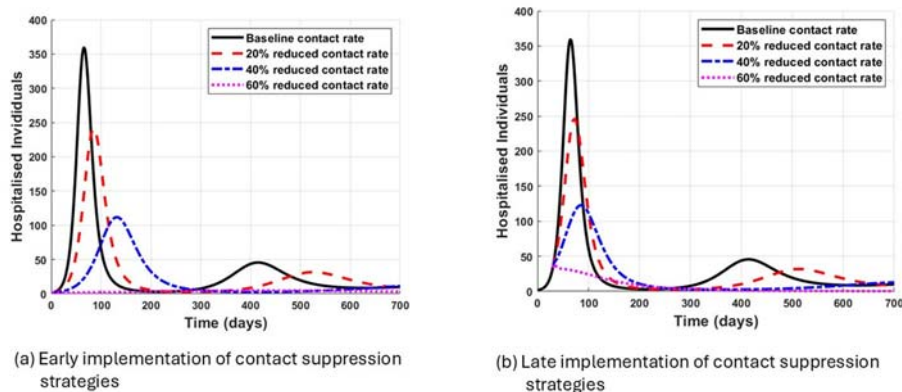


FIGURE 12

Shows the effect of (a) early implementation of contact suppression strategies, (b) late implementation of contact suppression strategies on the hospitalized population. Early implementation of strategies result in lower peak values of hospitalisations.

measures were assessed, including (1) implementation of contact suppression measures, (2) consideration of screening and isolation for asymptomatic infected individuals, and (3) the case when immunity wanes/does not wane within the modeling time. Our results showed that;

1. When disease contact suppression measures are enhanced, the reproduction number and the peak values of the infected population reduced in equal proportion. With early implementation of the measures, the results show that the peak values are attained at a much later stage of the epidemic (delayed peaks). This scenario allows for the healthcare system to prepare for cases that may require hospitalization. When the disease suppression measures are delayed by a few days, the peak values of the number of cases are attained at around the same time as the baseline case. However, the peak values are higher than in the cases of early implementation of contact suppression measures.
2. When disease screening and isolation of asymptomatic individuals are to be enforced, reasonable changes in the peak values of isolated individuals are observed but to the other infected classes. In relation to the asymptomatic population, the

change in the values of reproduction numbers calculated for the different levels of screening were also not significant (see Table 6).

3. Implementation of mitigation measures that prolong immunity to the disease would not only curb occurrence of multiple waves of the outbreak, but also lead to early containment of the infection.

Based on the results of this study, it is recommended that intervention measures be introduced early on in the outbreak since it delays and lower the peaks of the outbreak thereby easing pressure on the healthcare system. In addition, it is suggested that public health policies should prioritize implementing contact suppression interventions as well as long-term solutions like vaccination with boosters that induce immunity to the disease instead of less effective labor-intensive isolation strategies.

We note that since natural immunity wanes over a short period of time, the modeling framework can be extended to account for multiple waves and seasonality that is exhibited by the disease most especially in regions that experience wintry weather. In addition, the disease affects different age groups with varying

levels of severity and infection patterns where the infants and elderly tend to be the most adversely affected groups. Therefore, the modeling framework can be extended to describe disease transmission in age-clusters to produce more comprehensive results. More still, given that the two strains RSV A and RSV B often co-circulate annually in affected populations, future research work may consider extending the models to capture this aspect. However, it should be noted that, in a given season, one subtype may be more dominant than the other. Other aspects that can be considered in future work include vaccination, optimal control and cost-effectiveness analysis of any identified feasible RSV mitigation measures.

Data availability statement

The original contributions presented in the study are included in the article/supplementary material, further inquiries can be directed to the corresponding author.

Author contributions

LR: Conceptualization, Data curation, Formal analysis, Methodology, Writing – original draft, Writing – review & editing. MS: Data curation, Formal analysis, Writing – review & editing. HN: Conceptualization, Formal analysis, Supervision, Writing – review & editing. ZN: Data curation, Formal analysis, Writing – review & editing.

Funding

The author(s) declared that financial support was not received for this work and/or its publication.

References

- Coultas JA, Smyth R, Openshaw PJ. Respiratory syncytial virus (RSV): a scourge from infancy to old age. *Thorax*. (2019) 74:986–93. doi: 10.1136/thoraxjnl-2018-212212
- Cantú-Flores K, Rivera-Alfaro G, Muñoz-Escalante JC, Noyola DE. Global distribution of respiratory syncytial virus A and B infections: a systematic review. *Pathog Glob Health*. (2022) 116:398–409. doi: 10.1080/20477724.2022.2038053
- Ruckwardt TJ, Morabito KM, Graham BS. Determinants of early life immune responses to RSV infection. *Curr Opin Virol*. (2016) 16:151–7. doi: 10.1016/j.coviro.2016.01.003
- WHO. *Respiratory syncytial virus (RSV)* (2025). Available online at: [https://www.who.int/news-room/fact-sheets/detail/respiratory-syncytial-virus-\(rsv\)](https://www.who.int/news-room/fact-sheets/detail/respiratory-syncytial-virus-(rsv)) (Accessed February 3, 2025).
- Zhang L, Peeples ME, Boucher RC, Collins PL, Pickles RJ. Respiratory syncytial virus infection of human airway epithelial cells is polarized, specific to ciliated cells, and without obvious cytopathology. *J Virol*. (2002) 76:5654–66. doi: 10.1128/JVI.76.11.5654-5666.2002
- CDC. *Respiratory Syncytial Virus Infection (RSV): Symptoms and Care* (2023). Available online at: https://www.cdc.gov/rsv/about/?CDC_AAref_Val=https://www.cdc.gov/rsv/about/symptoms.html (Accessed February 3, 2025).
- MedlinePlus. *Respiratory Syncytial Virus Infections*. (2024). Available online at: <https://medlineplus.gov/respiratorysyncytialvirusinfections.html>
- Munywoki PK, Koech DC, Agoti CN, Bett A, Cane PA, Medley GF, et al. Frequent asymptomatic respiratory syncytial virus infections during an epidemic in a rural kenyan household cohort. *J Infect Dis*. (2015) 212:1711–8. doi: 10.1093/infdis/jiv263
- Martcheva M. *An introduction to Mathematical Epidemiology*. New York: Springer. (2015). doi: 10.1007/978-1-4899-7612-3
- Diekmann O, Heesterbeek JAP. *Mathematical Epidemiology of Infectious Diseases: Model Building, Analysis and Interpretation*. Baffins lane, Chichester, England: John Wiley & Sons, LTD. (2000).
- Pohjolainen S, Heiliö M, Lähivaara T, Laitinen E, Mantere T, Merikoski J, et al. *Mathematical Modelling*. Switzerland: Springer International Publishing (2016).
- Acedo L, Diez-Domongo J, Moraño JA, Villanueva RJ. Mathematical modelling of respiratory syncytial virus (RSV): vaccination strategies and budget applications. *Epidemiol Infect*. (2010) 138, 853–860. doi: 10.1017/S0950268809991373
- Halasa NB, Williams JV, G J Wilson WFW, Schaffner W, Wright PF. Medical and economic impact of a respiratory syncytial virus outbreak in a neonatal intensive care unit. *Pediatr Infect Dis J*. (2005) 24:1040–4. doi: 10.1097/01.inf.0000190027.59795.ac
- Weber A, Weber M, Milligan P. Modeling epidemics caused by respiratory syncytial virus (RSV). *Math Biosci*. (2001) 172:95–113. doi: 10.1016/S0025-5564(01)00066-9

Acknowledgments

LR and HN acknowledges the support from the Department of Mathematics and Statistical Sciences, BIUST. MS acknowledges the support of the Organization for Women in Science for the Developing World (OWSD) and the Swedish International Development Cooperation Agency (SIDA).

Conflict of interest

The author(s) declared that this work was conducted in the absence of any commercial or financial relationships that could be construed as a potential conflict of interest.

Generative AI statement

The author(s) declared that generative AI was not used in the creation of this manuscript.

Any alternative text (alt text) provided alongside figures in this article has been generated by Frontiers with the support of artificial intelligence and reasonable efforts have been made to ensure accuracy, including review by the authors wherever possible. If you identify any issues, please contact us.

Publisher's note

All claims expressed in this article are solely those of the authors and do not necessarily represent those of their affiliated organizations, or those of the publisher, the editors and the reviewers. Any product that may be evaluated in this article, or claim that may be made by its manufacturer, is not guaranteed or endorsed by the publisher.

15. Zhang H, Zhu A, Gao GF, Li Z. Epidemiological and clinical characteristics of respiratory syncytial virus infections in children aged < 5 years in China, from 2014-2018. *Vaccines*. (2022) 10:810. doi: 10.3390/vaccines10050810
16. Gov of Canada. *Respiratory syncytial virus: Infectious substances pathogen safety data sheet* (2026). Available online at: <https://www.canada.ca/en/public-health/services/laboratory-biosafety-biosecurity/pathogen-safety-data-sheets-risk-assessment/respiratory-syncytial-virus.html> (Accessed January 26, 2026).
17. Heywood AL. *Is It Possible to Get RSV More Than Once?* (2024). Available online at: <https://www.healthline.com/health/can-you-get-rsv-twice#takeaway> (Accessed March 27, 2024).
18. Bont L, Versteegh J, Swelsen W, Heijnen CJ, Kavelaars A, Brus F, et al. Natural reinfection with respiratory syncytial virus does not boost virus-specific t-cell immunity. *Pediatr Res*. (2002) 52:363-7. doi: 10.1203/00006450-200209000-00009
19. Terefe YA, Kassa SM, Njagarah JBH. Impact of the WHO integrated stewardship policy on the control of methicillin-resistant *Staphylococcus aureus* and third-generation cephalosporin-resistant *Escherichia coli*: using a mathematical modeling approach. *Bull Math Biol*. (2022) 84:97. doi: 10.1007/s11538-022-01051-1
20. Njagarah HJB, Nyabadza F. Modeling the impact of rehabilitation, amelioration and relapse on the prevalence of drug epidemics. *J Biol Dyn*. (2013) 21:1350001. doi: 10.1142/S0218339013500010
21. Sigauke M, Njagarah HJB, Kassa SM, Szomolay B. Can community-base care and environmental disinfection mitigate the pneumonia burden? *J Biol Syst*. (2025) 33:2550018. doi: 10.1142/S0218339025500184
22. van den Driessche P, Watmough J. Reproduction numbers and sub-threshold, endemic equilibria for compartmental models of disease transmission. *Math Biosci*. (2002) 180:29-48. doi: 10.1016/S0025-5564(02)00108-6
23. LaSalle JP. *The Stability of Dynamical Systems*. Philadelphia: Society for Industrial and Applied Mathematics. (1976).
24. Nyabadza F, Njagarah HJB, Smith RJ. Modelling the dynamics of crystal meth ('tik') abuse in the presence of drug-supply chains in South Africa. *Bull Math Biol*. (2013) 75:24-48. doi: 10.1007/s11538-012-9790-5
25. Kaler J, Hussain A, Patel K, Hernandez T, Ray S. Respiratory syncytial virus: a comprehensive review of transmission, pathophysiology, and manifestation. *Cureus*. (2023) 15:e36342. doi: 10.7759/cureus.36342
26. Blower SM, Dowlatabadi H. Sensitivity and uncertainty analysis of complex models of disease transmission: an HIV model, as an example. *Int Stat Rev*. (1994) 62:229-43. doi: 10.2307/1403510
27. Kassa SM, Njagarah JBH, Terefe YA. Analysis of the mitigation strategies for COVID-19: from mathematical modelling perspective. *Chaos, Solit Fractals*. (2020) 138:109968. doi: 10.1016/j.chaos.2020.109968
28. Government of Canada. *Respiratory syncytial virus (RSV): Prevention and risks*. (2024). Available online at: <https://www.canada.ca/en/public-health/services/diseases/respiratory-syncytial-virus-rsv/prevention-risks.html> (Accessed February 26, 2025).
29. Cohen C, Kleynhans J, Moyes J, McMorrow ML, Treurnicht FK, Hellferscee O, et al. Incidence and transmission of respiratory syncytial virus in urban and rural South Africa, 2017-2018. *Nat Commun*. (2024) 15:116. doi: 10.1038/s41467-023-44275-y
30. O'Neill A. *Sub-Saharan Africa: Life expectancy at birth from 2011 to 2021* (2024). Available online at: <https://www.statista.com/statistics/805644/life-expectancy-at-birth-in-sub-saharan-africa/> (Accessed June 20, 2024).
31. Havers FP, Whitaker M, Melgar M, Chatwani B, Chai SJ, Alden NB, et al. *Characteristics and Outcomes Among Adults Aged \geq 60 Years Hospitalized with Laboratory-Confirmed Respiratory Syncytial Virus-RSV-NET, 12 States, July 2022-June 2023*. (2024). Available online at: <https://www.cdc.gov/mmwr/volumes/72/wr/mm7240a1.htm> (Accessed May 2, 2024).